

Prediction of a novel topological multidefect ground state

Sergey Prosandeev,^{1,2} S. Prokhorenko,¹ Y. Nahas,¹ and L. Bellaïche¹

¹*Physics Department and Institute for Nanoscience and Engineering, University of Arkansas, Fayetteville, Arkansas 72701, USA*

²*Institute of Physics and Physics Department of Southern Federal University, Rostov-na-Donu 344090, Russia*



(Received 23 April 2019; published 28 October 2019)

Atomistic first-principles-based effective Hamiltonian simulations are conducted in some ferroelectric systems to predict the existence of a novel topological state. Such state is coined here as “topological eclecton” because it is made of a plethora of electrical topological defects, including (i) vortices and antivortices in different planes, (ii) hedgehogs and antihedgehogs, and (iii) a few skyrmions. Such state can be a ground state and readapt itself to form other striking topological states or phases when, e.g., heating the system or applying electric fields. In addition to its unique combined topological characteristics, it is also ferroelectric and chiral in nature.

DOI: [10.1103/PhysRevB.100.140104](https://doi.org/10.1103/PhysRevB.100.140104)

Various topological defects have been discovered in past decades in different materials, which led to a deepening of topology in condensed matter [1,2] and to the design of novel devices [3–6]. For instance, in *magnetic* systems, vortices [6], antivortices [7], bubbles [4], bobbers [8,9], merons, and skyrmions [10], were observed and predicted. Similarly, *electrical* vortices [11,12], antivortices [13], bubbles [14,15], dipolar waves [16,17], merons [17], and skyrmions [18,19] have been recently found in ferroelectrics. Striking phenomena can also result when *different* topological defects coexist within the same state or phase, as, e.g., evidenced by the Berezinskii-Kosterlitz-Thouless phase possessing both vortices and antivortices [20–27]. Such complex topological defects can be also created in, e.g., nanodimers made of two spheres [28]. Another example is the prediction of creating spontaneously optically active materials when both electrical vortices and antivortices form [29].

Based on such facts and the existence of, e.g., the Schlieren textures of nematic liquid crystals that contain different types of topological defects (such as boojums and disclinations [30,31]), one can wonder if presently unknown states or phases possessing a *variety* of topological defects await to be discovered in dipolar systems. The aim of this Rapid Communication is to reveal that it is the case. As a matter of fact, we discover (in some ferroelectric system) a novel state that we coin as “topological eclecton,” because of the eclectic occurrence of different vortices and antivortices, hedgehogs and antihedgehogs, and a few skyrmions. Such “topological eclecton” is presently found to be a *ground state*, and can generate other multidefect states and phases when under external knobs, such as temperature and fields. It also possesses a spontaneous electric polarization and is chiral, which further emphasizes its potential.

We employ here the effective Hamiltonian that was applied to $\text{Ba}_x\text{Sr}_{1-x}\text{TiO}_3$ solid solutions [32] and compositionally graded systems [33], as well as to $\text{BaTiO}_3/\text{SrTiO}_3$ superlattices [34,35] and nanocomposites [13,18,36–39]. It reproduces some experimental data, such as the critical transition temperatures in $\text{Ba}_{0.5}\text{Sr}_{0.5}\text{TiO}_3$ disordered alloys [32] and the phenomenon and even magnitude of the temperature-gradient-

induced polarization in $\text{Ba}_{0.75}\text{Sr}_{0.25}\text{O}_3$ [40]. Effective Hamiltonian techniques have played a major role in the field of electrical topological defects by predicting electrical vortices [11], bubbles [14], dipolar waves [16], and skyrmions [18], that have then been experimentally confirmed [12,15,17,19].

Here, we select $24 \times 24 \times 12$ supercells that are periodic along all Cartesian directions, and inside which two BaTiO_3 (BTO) conical nanostructures are embedded in a SrTiO_3 (STO) matrix [STO should, in fact, be considered to be $(\text{Ba}_{0.15}\text{Sr}_{0.85})\text{O}_3$ here since our effective Hamiltonian predicts a paraelectric-to-ferroelectric transition of about 100 K in STO [32]]. These two cones are inverted with respect to each other, are connected to each other by their tips, and each have a radius of 33 Å for their common (x, y) base and a height (along the z axis) of 23 Å (the x , y , and z axes are along the pseudocubic [100], [010], and [001] directions). Such nanostructure is reminiscent of InAs pyramidlike structures occurring inside a GaAs matrix [41,42], and of chains made of semiconductor quantum dots [43–47].

Our effective Hamiltonian is used within Monte Carlo (MC) simulations by cooling the system. 20 000 MC sweeps are employed to equilibrate the system at each temperature, and then another 20 000 sweeps are used to compute thermodynamical averages. A particular output of simulations consists of the patterns of local modes (that are proportional to local electric dipoles) at each five-atom site i , to be denoted by \mathbf{u}_i , at each MC sweep. Another extracted quantity is the toroidal moment of the local modes [48]:

$$\mathbf{G} = \left\langle \frac{1}{2N} \sum_i \mathbf{r}_i \times (\mathbf{u}_i - \langle \mathbf{u} \rangle) \right\rangle, \quad (1)$$

where $\langle \mathbf{u} \rangle$ is the supercell average over the local modes, \mathbf{r}_i is the position vector locating the i th site, and N is the number of sites.

We also obtain generalized quadrupole moments of the density matrix [49]:

$$Q_{\alpha\beta} = \left\langle \frac{1}{2N} \sum_i (3r_{i\alpha}r_{i\beta} - r_i^2\delta_{\alpha\beta})\rho_{i\alpha\beta} \right\rangle, \quad (2)$$

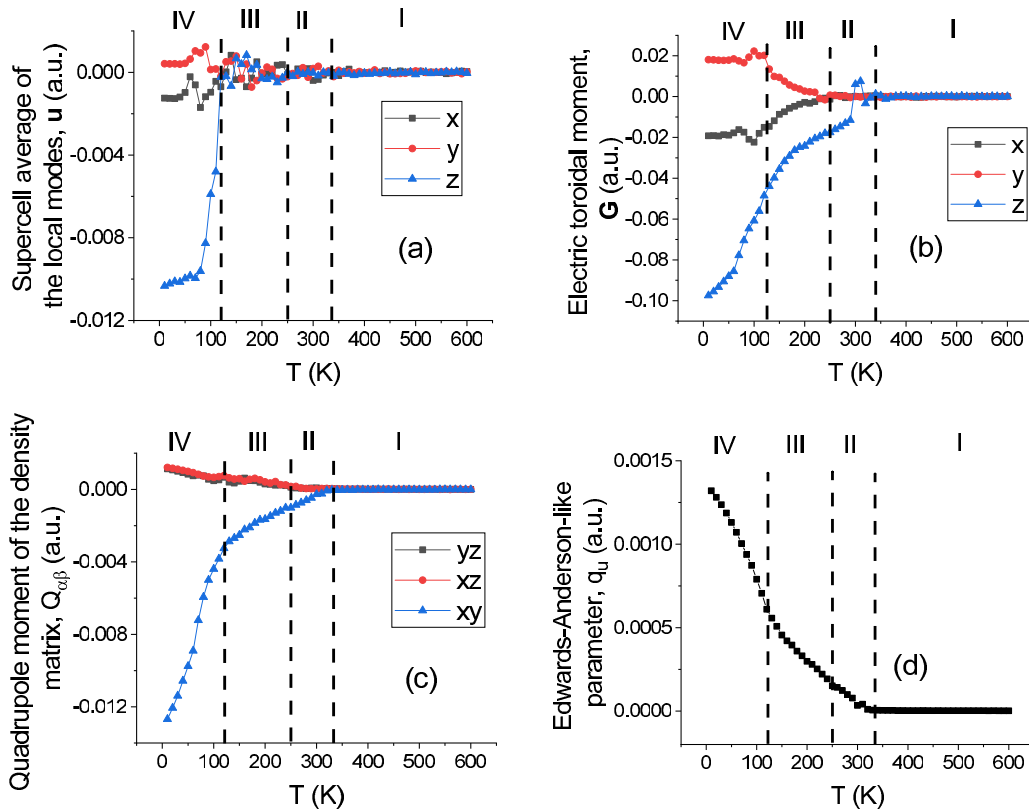


FIG. 1. Macroscopic quantities obtained on cooling the investigated system as a function of temperature: (a) supercell average of the local modes; (b) electric toroidal moment; (c) quadrupole moment of the density; and (d) Edwards-Anderson-like parameter. Note that error bars in our low-temperature calculations are smaller than the size of the symbols.

where $\delta_{\alpha\beta}$ is the Kronecker symbol while $\rho_{i\alpha\beta} = (u_{i\alpha} - \langle u_{\alpha} \rangle)(u_{i\beta} - \langle u_{\beta} \rangle)$.

An Edwards-Anderson-like parameter is also determined as [50]

$$q_u = \frac{1}{N} \sum_i \sum_{\alpha} \langle (u_{i\alpha} - \langle u_{\alpha} \rangle)^2 \rangle. \quad (3)$$

Quantities of Eqs. (1)–(3) will help in identifying different phases.

Figure 1 reports these calculated quantities and the supercell average of the local modes (that is proportional to the electrical polarization), for the investigated system on cooling from 600 to 10 K with a step of 10 K. Figure 2 shows the projection of the pattern of the local modes into specific planes, as averaged over the last 20 000 MC sweeps for some temperatures, T .

The system is paraelectric and paratoroidic for T above $\simeq 340$ K since $\langle \mathbf{u} \rangle$ and \mathbf{G} both vanish there, in addition to the $Q_{\alpha\beta}$'s and q_u annihilating too. Such region is denoted as phase I. Upon cooling, another phase, to be coined phase II, appears and extends from $\simeq 340$ to about 250 K. Phase II is characterized by the z component of the toroidal moment getting finite, along with the Q_{xy} element of the density matrix and q_u also now deviating from zero, with these quantities strengthening in magnitude when decreasing T within phase II. Such nonzero quantities reflect the emergence of electric vortices in (x, y) planes, as evidenced in Fig. 2(c) for the basal plane ($Z = 1$) of BTO cones, therefore making phase II

ferrotoroidic. We therefore predict a phase transformation from paratoroidic to ferrotoroidic at $\simeq 340$ K. There is also no evident dipolar ordering in the (x, z) and (y, z) planes in phase II, as indicated by the small and disordered arrows in Figs. 2(a) and 2(b).

Another transition occurs at about 250 K from phase II to a new phase that we denote as phase III. This latter phase is associated with the x and y components of the toroidal moment and the Q_{xz} and Q_{yz} quadrupoles all becoming finite. Phase III ranges from 250 to $\simeq 120$ K. The emergence of such finite quantities point out that, in addition to a persistent electrical vortex in the (x, y) basal planes [see Fig. 2(f)], another dipolar ordering is emerging in other planes. This is demonstrated by Figs. 2(d) and 2(e) revealing the existence of vortices lying in some (x, z) and (y, z) planes and made by two half-vortices, each located within adjacent BTO cones that are connected by the same base (half-vortices have been reported in magnetic systems [51]). Furthermore, the fact that other adjacent cones are connected by their tip in our supercell has another topological implication in both (x, z) and (y, z) planes: such successive cones experience an antivortex type of configuration near such tip [see circles in Figs. 2(d) and 2(e)]. Phase III can therefore be described as made of interconnected chains of vortices and antivortices in the (x, z) and (y, z) planes passing through the tip, along with dipole vortices in the (x, y) basal planes. We are not aware of any previous determination of such phase.

Upon further cooling, the average local mode adopts a z component that becomes finite below $\simeq 120$ K, along with x

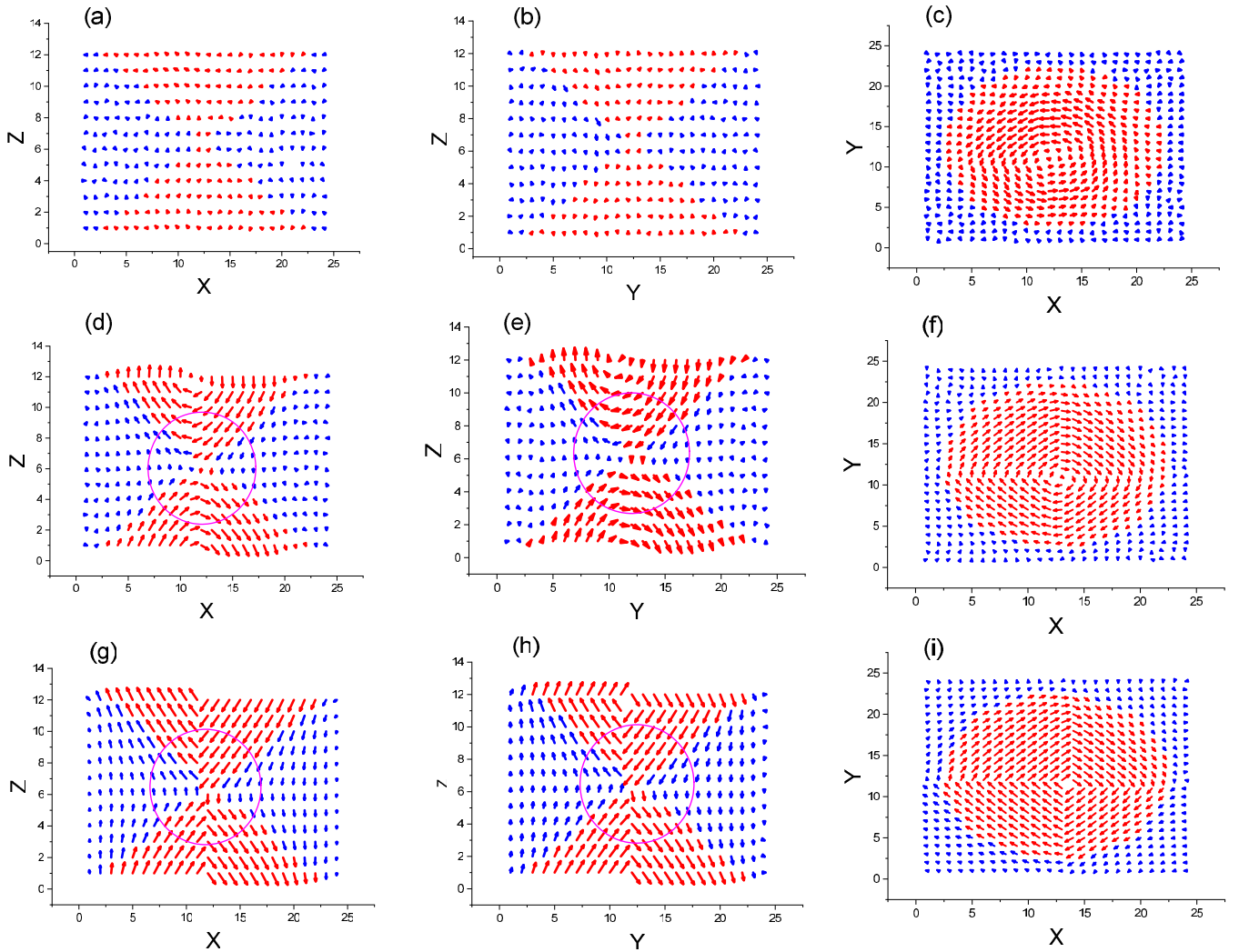


FIG. 2. Dipolar patterns in the (x, z) plane defined by $y = 12$, (y, z) plane defined by $x = 12$ and the (x, y) plane defined by $z = 1$ (and that corresponds to a basal plane of a BTO cone), as obtained at (a)–(c) 300 K (phase II); (d)–(f) 200 K (phase III); and (g)–(i) 10 K (phase IV), when cooling the investigated system. The center of the large magenta circles of panels (d), (e), (g), and (h) corresponds to the core of an antivortex. The red color marks the Ti-centered dipoles at sites i for which the associated A sites i are inside the BTO cones, while the blue color refers to Ti-centered dipoles at sites i for which the associated A sites i are located inside the STO matrix.

and y components getting also finite but smaller in magnitude and of opposite signs between each other [see Fig. 1(a)]. This marks the emergence of a new phase coined as phase IV and that, unlike phase III, possesses a spontaneous polarization, therefore making phase IV ferrotoroidic and ferroelectric. The x , y , and especially the z axis adopt both a finite component of the toroidal moment and of the polarization, which make phase IV chiral in nature [11, 18, 39, 52, 53] and further emphasizes its potential applications. The x and y components of the toroidal moment are nearly independent of the temperature in phase IV [see Fig. 1(b)]. The corresponding dipolar patterns of phase IV are shown in Figs. 2(g)–2(i). The electric vortex in the (x, y) basal plane shown in Fig. 2(i) can now be considered to be made of four 90° domains rather than being circular as in phases II and III, with the vortex core having slightly shifted with respect to the center of the base (because of the small in-plane electrical polarization). Moreover, Figs. 2(g) and 2(h) indicate that the appearance of a spontaneous polarization along the z axis has rendered the half-

vortices being asymmetric with respect to the z line passing through the tips of the cone and also being less circular in shape [the z component of the dipoles suddenly change sign along the x or y axis within the cones in Fig. 2(g) and 2(h), while the evolution of this component was more gradual in Figs. 2(d) and 2(e)]. The STO matrix has become polarized along the z axis in phase IV with up and down domains alternating along the y axis in the (y, z) plane with the alternation taking place in the sites that are located halfway (along the y axis) between two successive rows of BTO cones, as evidenced by periodically repeating the pattern of Fig. 2(h) along the y axis. Similar symmetrical features occur in the STO matrix in the (x, z) plane and along the x axis [see Fig. 2(g)].

To further describe phase IV at low temperature, we carried out topological characterization of its dipolar patterns at 10 K. We computed several types of topological charges: (i) $S_1 \rightarrow S_1$ (circle to circle) winding number used to identify vortex- and anti-vortex-type point defects [2]; (ii) $S_2 \rightarrow S_2$

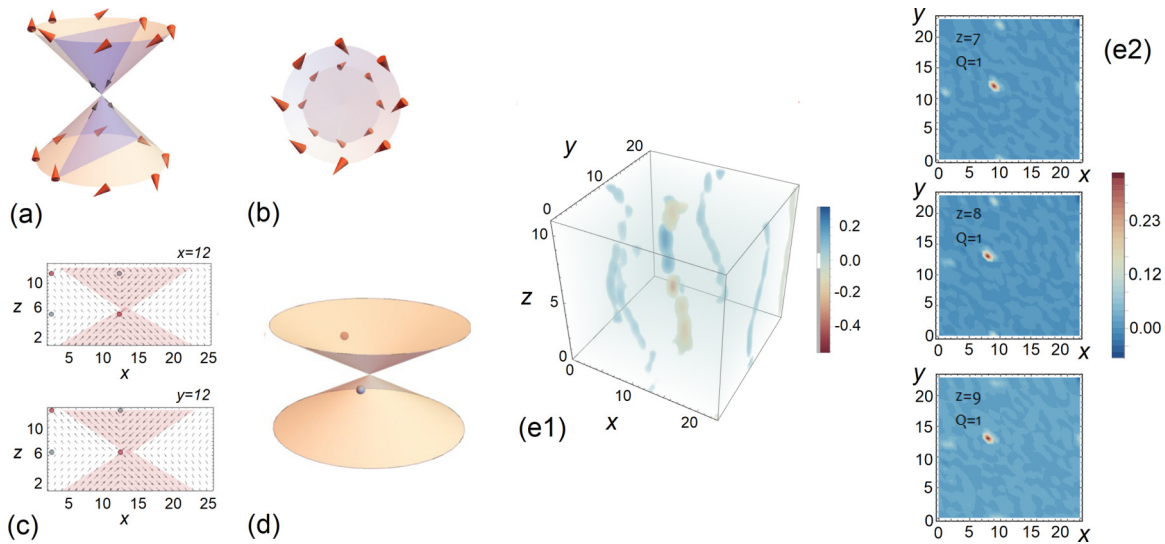


FIG. 3. Dipolar structure and topology of the “topological eclectic” at 10 K. Panels (a) and (b) show a schematization of the dipolar structure. Panel (a) corresponds to a general viewpoint position while panel (b) depicts the top view from the z axis (due to perspective, the circle corresponding to the lower cone base appears to have a smaller diameter than that of the upper cone base). In both panels (a) and (b), orange arrows indicate the orientation of the dipoles on the outer surfaces of the cones. The blue triangle in panel (a) shows a (y, z) cross section of the cones passing through the revolution axis. The in-plane projection of the dipoles located at this cross section exhibits an antivortex at the meeting point of the cone tips schematically indicated by small black arrows in panel (a). A complete projection plot within the (y, z) and (x, z) planes passing through the center of the cones is shown in panel (c) where vortex and antivortex cores are indicated with blue and red circles, respectively. Panel (d) shows the location of hedgehog (red sphere) and antihedgehog (blue sphere) point defects. Panel (e1) shows the distribution of the Pontryagin charge density within the (x, y) planes in the full supercell. Panels (e2) show the Pontryagin charge density distribution in the three (x, y) planes that host skyrmions.

(sphere to sphere) winding number enabling the mapping of three-dimensional point defects such as hedgehogs and antihedgehogs [2]; and finally (iii) $D_1 \rightarrow S_2$ (disk to sphere) Pontryagin’s or skyrmion charge [54].

Results are displayed in Figs. 3(a)–3(e), via schematization. Figure 3(c) confirms the presence of antivortices with their core being located at the meeting points of the cone tips in the (x, z) and (y, z) planes and of vortices with their core occurring inside the BTO cones at the meeting plane of the bases of such cones. The left side of the two snapshots of Fig. 3(c) also indicates other vortices and antivortices inside the STO matrix within the (y, z) and (x, z) planes. Furthermore, phase IV at low temperature possesses hedgehog-antihedgehog pairs [see Fig. 3(d)]. Interestingly, the hedgehog lies in close vicinity of the cones’ tips: the center of the hedgehog is located at (12.5, 10.5, 5.5) in our (x, y, z) basis while the tip of the cone sits at (12.5, 12.5, 6.5). This hedgehog is somehow reminiscent of the Bloch point reported in the magnetic bobber [9] since both the hedgehog and the Bloch point carry a +1 point topological charge in three dimensions [55]. However, and unlike the magnetic bobber, phase IV at low temperature only possesses skyrmions in some of its (x, y) planes, that are, in fact, located between the two (x, y) planes hosting the hedgehog and antihedgehog topological defects [the center of the antihedgehog is located at (8.5, 14.5, 9.5) in our (x, y, z) basis]. Figures 3(e1) and 3(e2) show the distribution of the Pontryagin charge density within the (x, y) planes in the full supercell and in those middle (x, y) planes (defined by $z = 7, 8,$ and 9) hosting skyrmions, respectively. In these middle planes, the +1 skyrmionic charge is almost completely localized [see Fig. 3(e2)] at the junction of domain walls

reversing the sign of the x and y polarization components that yields the “central” vortex in the (x, y) planes, inside the BTO cone [see Fig. 2(i)]. The remainder of the skyrmionic charge in the (x, y) planes is located at the supercell boundaries inside of the STO matrix [see Figs. 2(i) and 3(e2)].

Phase IV thus harbors at low temperature a state that is endowed with a novel and exotic topological structure. We name it “topological eclectic” with regard to its “eclectic” topological nature made of vortices, antivortices, hedgehog, antihedgehog, and a few skyrmions. Such new and *ground* state may be of importance to design new types of nonvolatile memory devices. Interestingly, phases possessing different topological defects are already known in several types of materials, but they are usually made of “only” two opposite such defects, such as (i) vortices and antivortices making the so-called phase-locked state [13,56], or creating a gyrotropic state in some materials [29], or even being ingredients of the Berezinskii-Kosterlitz-Thouless phase [20–27]; and (ii) hedgehog and antihedgehog, extensively discussed in liquid crystals [57], cosmology [58], but also in ferroelectrics [59,60]. It will also be interesting in the future to reveal how these various topological defects interact with each other when under an ac probe, and likely yield unusual dynamical features [38,54,61].

Note also that phase III can be considered to be a modification of the topological eclectic since we, e.g., numerically find that increasing the temperature disorganizes the structure, leading to a proliferation of hedgehogs and antihedgehogs, as well as small vortices and antivortices in (x, z) and (y, z) planes. Starting from this “topological eclectic” and *applying some external factors* can also result in other striking

topological states and phases. For instance, yet another topologically nontrivial state, that is, a “skyrmionic tube,” can emerge from the topological eclectic upon application of an external electric field. This skyrmionic tube state is also composed of many topological defects and is topologically similar to that of Ref. [18] (see Supplemental Material [62], and references therein [18,39,52–54,63]).

In summary, we predict a novel topological state coined here “topological eclectic” and simultaneously possessing vortices, antivortices, hedgehogs, antihedgehogs, and a few skyrmions. This “topological eclectic” is the ground state of the studied nanostructure [64], and is chiral in nature. It can also transform to other complex topological states and phases via the application of, e.g., temperature and fields. Note that we used here specific shapes (e.g., inverted cones) of a ferroelectric nanocomposite to make such state “easily” appear, by creating a specific depolarizing electric field [11,14,18,37,39,65–69]. However, other types of ferroelectric nanostructures may also host the “topological eclectic,” since we previously predicted an electric skyrmion in

another nanocomposite [18] while it was then predicted in the simple PbTiO_3 material [70] and observed in ferroelectric superlattices [19]. We also hope that our study will encourage varying the shape of ferroelectric nanostructures to discover novel topological phases as well as open a research field dedicated to studying interaction of various topological defects within the same phase. The “topological eclectic” may also exist in other types of materials (e.g., magnets, superfluids, and superconductors) because of the existence of other interactions there that also favor the emergence of topological defects (such as Dzyaloshinskii-Moriya interactions [71] in magnets).

This work is supported by the DARPA Grant No. HR0011727183-D18AP00010 (TEE Program). L.B. acknowledges discussion with Professor Blügel. Sergey P. appreciates the support of Russian Ministry of Science and Higher Education 3.1649.2017/4.6 and RFBR 18-52-00029_Bel_a. Sergey P. and L.B. also acknowledge ONR Grant No. N00014-17-1-2818.

-
- [1] *Topology and Geometry in Physics*, edited by E. Bick and F. D. Steffen, Lecture Notes in Physics Vol. 659 (Springer, Berlin/Heidelberg, 2005).
- [2] N. D. Mermin, *Mod. Phys.* **51**, 591 (1979).
- [3] J. Zhang, M. T. Albelda, Y. Liu, and J. W. Canary, *Chirality* **17**, 404 (2005).
- [4] M. Prakash and N. Gershenfeld, *Science* **315**, 832 (2007).
- [5] Y. Huang, W. Kang, X. Zhang, Y. Zhou, and W. Zhao, *Nanotechnology* **28**, 08LT02 (2017).
- [6] S. D. Bader, *Rev. Mod. Phys.* **78**, 1 (2006).
- [7] K. Shigeto, T. Okuno, K. Mibu, T. Shinjo, and T. Ono, *Appl. Phys. Lett.* **80**, 4190 (2002).
- [8] F. Zheng, F. N. Rybakov, A. B. Borisov, D. Song, S. Wang, Z.-A. Li, H. Du, N. S. Kiselev, J. Caron, A. Kovács, M. Tian, Y. Zhang, S. Blügel, and R. E. Dunin-Borkowski, *Nat. Nanotechnol.* **13**, 451 (2018).
- [9] F. N. Rybakov, A. B. Borisov, S. Blügel, and N. S. Kiselev, *Phys. Rev. Lett.* **115**, 117201 (2015).
- [10] X. Z. Yu, W. Koshibae, Y. Tokunaga, K. Shibata, Y. Taguchi, N. Nagaosa, and Y. Tokura, *Nature (London)* **564**, 95 (2018).
- [11] I. Naumov, L. Bellaiche, and H. Fu, *Nature (London)* **432**, 737 (2004).
- [12] A. K. Yadav, C. T. Nelson, S. L. Hsu, Z. Hong, J. D. Clarkson, C. M. Schlepütz, A. R. Damodaran, P. Shafer, E. Arenholz, L. R. Dedon, D. Chen, A. Vishwanath, A. M. Minor, L. Q. Chen, J. F. Scott, L. W. Martin, and R. Ramesh, *Nature (London)* **530**, 198 (2016).
- [13] L. Louis, I. Kornev, G. Geneste, B. Dkhil, and L. Bellaiche, *J. Phys.: Condens. Matter* **24**, 402201 (2012).
- [14] B.-K. Lai, I. Ponomareva, I. I. Naumov, I. A. Kornev, H. Fu, L. Bellaiche, and G. J. Salamo, *Phys. Rev. Lett.* **96**, 137602 (2006).
- [15] Q. Zhang, L. Xie, G. Liu, S. Prokhorenko, Y. Nahas, X. Pan, L. Bellaiche, A. Gruverman, and N. Valanoor, *Adv. Mater.* **29**, 1702375 (2017).
- [16] D. Sichega and L. Bellaiche, *Phys. Rev. Lett.* **106**, 196102 (2011).
- [17] L. Lu, Y. Nahas, M. Liu, H. Du, Z. Jiang, S. Ren, D. Wang, L. Jin, S. Prokhorenko, C.-L. Jia, and L. Bellaiche, *Phys. Rev. Lett.* **120**, 177601 (2018).
- [18] Y. Nahas, S. Prokhorenko, L. Louis, Z. Gui, I. Kornev, and L. Bellaiche, *Nat. Commun.* **6**, 8542 (2015).
- [19] S. Das, Y. L. Tang, Z. Hong, M. A. P. Gonçalves, M. R. McCarter, C. Klewe, K. X. Nguyen, F. Gomez-Ortiz, P. Shafer, E. Arenholz, V. A. Stoica, S.-L. Hsu, B. Wang, C. Ophus, J. F. Liu, C. T. Nelson, S. Saremi, B. Prasad, A. B. Mei, D. G. Schlom, J. Íñiguez *et al.*, *Nature (London)* **568**, 368 (2019).
- [20] Y. Nahas, S. Prokhorenko, I. Kornev, and L. Bellaiche, *Phys. Rev. Lett.* **119**, 117601 (2017).
- [21] D. J. Bishop and J. D. Reppy, *Phys. Rev. Lett.* **40**, 1727 (1978).
- [22] M. R. Beasley, J. E. Mooij, and T. P. Orlando, *Phys. Rev. Lett.* **42**, 1165 (1979).
- [23] A. F. Hebard and A. T. Fiory, *Phys. Rev. Lett.* **44**, 291 (1980).
- [24] S. A. Wolf, D. U. Gubser, W. W. Fuller, J. C. Garland, and R. S. Newrock, *Phys. Rev. Lett.* **47**, 1071 (1981).
- [25] J. Fröhlich and T. Spencer, *Commun. Math. Phys.* **81**, 527 (1981).
- [26] D. J. Resnick, J. C. Garland, J. T. Boyd, S. Shoemaker, and R. S. Newrock, *Phys. Rev. Lett.* **47**, 1542 (1981).
- [27] P. E. Lammert, D. S. Rokhsar, and J. Toner, *Phys. Rev. Lett.* **70**, 1650 (1993).
- [28] J. Mangeri, S. P. Alpay, S. Nakhmanson, and O. G. Heinonen, *Appl. Phys. Lett.* **113**, 092901 (2018).
- [29] S. Prosandeev, I. A. Kornev, and L. Bellaiche, *Phys. Rev. Lett.* **107**, 117602 (2011).
- [30] P. G. de Gennes, *The Physics of Liquid Crystals*, 2nd ed. (Clarendon, Oxford, 1993).
- [31] S. Chandrasekhar, *Liquid Crystals* (Cambridge University Press, Cambridge, 1977).

- [32] L. Walizer, S. Lisenkov, and L. Bellaiche, *Phys. Rev. B* **73**, 144105 (2006).
- [33] N. Choudhury, L. Walizer, S. Lisenkov, and L. Bellaiche, *Nature (London)* **470**, 513 (2011).
- [34] S. Lisenkov and L. Bellaiche, *Phys. Rev. B* **76**, 020102(R) (2007).
- [35] S. Lisenkov, I. Ponomareva, and L. Bellaiche, *Phys. Rev. B* **79**, 024101 (2009).
- [36] Y. Nahas, S. Prokhorenko, and L. Bellaiche, *Phys. Rev. Lett.* **116**, 117603 (2016).
- [37] Z. Gui, L.-W. Wang, and L. Bellaiche, *Nano Lett.* **15**, 3224 (2015).
- [38] Z. Gui and L. Bellaiche, *Phys. Rev. B* **89**, 064303 (2014).
- [39] S. Prosandeev, A. Malashevich, Z. Gui, L. Louis, R. Walter, I. Souza, and L. Bellaiche, *Phys. Rev. B* **87**, 195111 (2013).
- [40] Q. Zhang and I. Ponomareva, *Phys. Rev. Lett.* **105**, 147602 (2010).
- [41] D. Bimberg, M. Grundmann, and N. N. Ledentsov, *Quantum Dot Heterostructures* (Wiley, New York, 1998).
- [42] D. M. Bruls, J. W. A. M. Vugs, P. M. Koenraad, H. W. M. Salemink, J. H. Wolter, M. Hopkinson, M. S. Skolnick, F. Long, and S. P. A. Gill, *Appl. Phys. Lett.* **81**, 1708 (2002).
- [43] Yu. I. Mazur, W. Q. Ma, X. Wang, Z. M. Wang, G. J. Salamo, M. Xiao, T. D. Mishima, and M. B. Johnson, *Appl. Phys. Lett.* **83**, 987 (2003).
- [44] Z. M. Wang, Yu. I. Mazur, G. J. Salamo, P. M. Lytvin, V. V. Strelchuk, and M. Ya. Valakh, *Appl. Phys. Lett.* **84**, 4681 (2004).
- [45] M. Schmidbauer, Sh. Seydmohamadi, D. Grigoriev, Zh. M. Wang, Yu. I. Mazur, P. Schäfer, M. Hanke, R. Köhler, and G. J. Salamo, *Phys. Rev. Lett.* **96**, 066108 (2006).
- [46] Z. M. Wang, K. Holmes, Yu. I. Mazur, and G. J. Salamo, *Appl. Phys. Lett.* **84**, 1931 (2004).
- [47] Zh. M. Wang, Yu. I. Mazur, J. L. Shultz, G. J. Salamo, T. D. Mishima, and M. B. Johnson, *J. Appl. Phys.* **99**, 033705 (2006).
- [48] S. Prosandeev and L. Bellaiche, *Phys. Rev. B* **77**, 060101(R) (2008).
- [49] D. J. Griffiths, *Introduction to Electrodynamics*, 4th ed. (Cambridge University Press, Boston, 2017).
- [50] S. Prosandeev, D. Wang, A. R. Akbarzadeh, and L. Bellaiche, *J. Phys.: Condens. Matter* **27**, 223202 (2015).
- [51] O. Tchernyshyov and G.-W. Chern, *Phys. Rev. Lett.* **95**, 197204 (2005).
- [52] P. Shafer, P. García-Fernández, P. Aguado-Puente, A. R. Damodaran, A. K. Yadav, C. T. Nelson, S.-L. Hsu, J. C. Wojdeł, J. Íñiguez, L. W. Martin, E. Arenholz, J. Junquera, and R. Ramesh, *Proc. Natl. Acad. Sci. USA* **115**, 915 (2018).
- [53] A. R. Damodaran, J. D. Clarkson, Z. Hong, H. Liu, A. K. Yadav, C. T. Nelson, S.-L. Hsu, M. R. McCarter, K.-D. Park, V. Kravtsov, A. Farhan, Y. Dong, Z. Cai, H. Zhou, P. Aguado-Puente, P. García-Fernández, J. Íñiguez, J. Junquera, A. Scholl, M. B. Raschke *et al.*, *Nat. Mater.* **16**, 1003 (2017).
- [54] N. Nagaosa and Y. Tokura, *Nat. Nanotechnol.* **8**, 899 (2013).
- [55] A. P. Malozemoff and J. C. Slonczewski, *Magnetic Domain Walls in Bubble Materials, 1st Edition*, in Advances in Materials and Device Research, edited by Raymond Wolfe (Academic Press, London, 1979).
- [56] A. Ruotolo, V. Cros, B. Georges, A. Dussaux, J. Grollier, C. Deranlot, R. Guillemet, K. Bouzehouane, S. Fusil, and A. Fert, *Nat. Nanotechnol.* **4**, 528 (2009).
- [57] T. C. Lubensky, D. Pettey, N. Carrier, and H. Stark, *Phys. Rev. E* **57**, 610 (1998).
- [58] A. Vilenkin and E. P. S. Shellard, *Cosmic Strings and Other Topological Defects* (Cambridge University Press, Cambridge, UK, 1994).
- [59] S. Prokhorenko, Y. Nahas, and L. Bellaiche, *Phys. Rev. Lett.* **118**, 147601 (2017).
- [60] Y. Nahas, S. Prokhorenko, I. Kornev, and L. Bellaiche, *Phys. Rev. Lett.* **116**, 127601 (2016).
- [61] C. Liu, J. Shen, and X. Yang, *Commun. Comput. Phys.* **2**, 1184 (2007).
- [62] See Supplemental Material at <http://link.aps.org/supplemental/10.1103/PhysRevB.100.140104> for the effect of the radius of the base of the BaTiO₃ cone on the ground state and for another interesting topological state (that is, the skyrmionic tube) that can be created from the “topological electron.”
- [63] B. Xu, J. Íñiguez, and L. Bellaiche, *Nat. Commun.* **8**, 15682 (2017).
- [64] Note that we slowly cooled down the system in order to reach the ground state, but also compared the energy of different phases obtained by various strategies at low temperature (such as applying an electric field to get new states and then conducting further full relaxation of such new states but now under no electric field).
- [65] M. G. Stachiotti and M. Sepiarsky, *Phys. Rev. Lett.* **106**, 137601 (2011).
- [66] S. Prosandeev and L. Bellaiche, *Phys. Rev. Lett.* **97**, 167601 (2006).
- [67] L. Lahoche, I. Luk’yanchuk, and G. Pascoli, *Integr. Ferroelectr.* **99**, 60 (2008).
- [68] I. Ponomareva, I. I. Naumov, and L. Bellaiche, *Phys. Rev. B* **72**, 214118 (2005).
- [69] A. P. Levanyuk and R. Blinc, *Phys. Rev. Lett.* **111**, 097601 (2013).
- [70] M. A. P. Gonçalves, C. Escorihuela-Sayalero, P. García-Fernández, J. Junquera, and J. Íñiguez, *Sci. Adv.* **5**, eaau7023/1-5 (2019).
- [71] I. Dzyaloshinskii, *J. Phys. Chem. Solids* **4**, 241 (1958); I. Dzyaloshinskii and T. Moriya, *Phys. Rev.* **120**, 91 (1960).